

Asian Power Electronics Journal

PERC, HK PolyU

Copyright © The Hong Kong Polytechnic University 2020. All right reserved.

No part of this publication may be reproduced or transmitted in any form or by any means, electronic or mechanical, including photocopying recording or any information storage or retrieval system, without permission in writing form the publisher.

First edition August 2020 Printed in Hong Kong by Reprographic Unit.
The Hong Kong Polytechnic University

Published by

Power Electronics Research Centre
The Hong Kong Polytechnic University
Hung Hom, Kowloon, Hong Kong

ISSN 1995-1051

Disclaimer

Any opinions, findings, conclusions, or recommendations expressed in this material/event do not reflect the views of The Hong Kong Polytechnic University

Editorial board

Honorary Editor

Prof. Fred C. Lee, Electrical and Computer Engineer, Virginia Polytechnic Institute and State University

Editor

Victor Electronic Ltd.

Associate Editors and Advisors

Prof. Philip T. Krien
Department of Electrical and Computer Engineering, University of Illinois

Prof. Keyue Smedley
Department of Electrical and Computer Engineering, University of California

Prof. Muhammad H. Rashid
Department of Electrical and Computer Engineering, University of West Florida

Prof. Dehong Xu
College of Electrical Engineering, Zhejiang University

Prof. Hirofumi Akagi
Department of Electrical Engineering, Tokyo Institute of Technology

Prof. Xiao-zhong Liao
Department of Automatic Control, Beijing Institute of Technology

Prof. Hao Chen
Department of Automation, China University of Mining and Technology

Prof. Danny Sutanto
Integral Energy Power Quality and Reliability Centre, University of Wollongong

Prof. S.L. Ho
Department of Electrical Engineering, The Hong Kong Polytechnic University

Prof. Eric K.W. Cheng
Department of Electrical Engineering, The Hong Kong Polytechnic University

Dr. Norbert C. Cheung
Department of Electrical Engineering, The Hong Kong Polytechnic University

Dr. Edward W.C. Lo
Department of Electrical Engineering, The Hong Kong Polytechnic University

Dr. Martin H. L. Chow
Department of Electrical Engineering, The Hong Kong Polytechnic University

Dr. Chi Kwan Lee
Department of Electrical and Electronic Engineering, The University of Hong Kong

Publishing Director:

Prof. Eric K.W. Cheng, Department of Electrical Engineering, The Hong Kong Polytechnic University

Communications and Development Director:

Dr. James H.F. Ho, Department of Electrical Engineering, The Hong Kong Polytechnic University

Production Coordinator

Dr. Jinghong Sun, Dr. Xiaolin Wang, and Dr. Zilin Li, Power Electronics Research Centre, The Hong Kong Polytechnic University

Secretary:

Ms. Kit Chan, Department of Electrical Engineering, The Hong Kong Polytechnic University

Table of Content

Adaptive Control of Quadrotor UAV Based on Arduino	1
Xiaodi Zhang	
Topology and Analysis of an Electromechanical Brake for Electric Vehicles	5
Xiangdang Xue, Ka Wai Eric Cheng, and Yulong Fan	
Research on Symmetrical Half-Bridge Switched Capacitor Active Equalization Circuit of Vehicle Power Lead-Acid Battery	10
Mingyu Gao, Jifeng Qu, Junfan Wang, Huipin Lin, Minghao Wang	
Author Index	15

Adaptive Control of Quadrotor UAV Based on Arduino

Xiaodi Zhang¹

¹School of Mechatronic Engineering and Automation, Shanghai University, Shanghai
E-mail: 18122806@shu.edu.cn

Abstract –This paper mainly studies the control of the sensors of the quadcopter unmanned aerial vehicle (UAV) based on the serial-stage PID controller. Firstly, by modeling the dynamic model of the drones, the control method of the quadcopter unmanned aerial vehicle is illustrated. After that, the design requirements for the parameters and precision of the sensors and executors needed in this design are put forward, and the device comparison is carried out. Finally, a system design scheme with four brushless DC motor speed control is given, and the scheme is tested.

Keywords – Adaptive control, manned aerial vehicle, circuit design, Arduino

I. INTRODUCTION

The four-rotor drone is used as a small, flexible, lightweight, portable underdrive system [1]. While rotary-wing drones do not require theoretical knowledge, such as overly complex aerodynamics compared with fixed-wing drones. They are less stringent than conventional helicopters in terms of blade and pitch. However, due to its multivariable, strong coupling characteristics, the real-time control is difficult.

Four-rotor unmanned aerial vehicle (UAV) achieves space six degrees of freedom movement through the distribution of control amount. However, due to the large vibration of the multi-motor operation, the large-angle maneuvering is often caused and serious misalignment of sensor data, the use of high-quality sensor components will significantly increase the overall cost increased. In addition, the higher requirements are also put forward for the multi-motor multi-propeller control parameters of the system also put forward. These factors limit the development of high-rotor drones.

Currently, the manufacturers have designed new flight control panels for in-flight executors and sensor failures. For example, CAUV adds a backup sensor in its own flight control board. The probability of accidents reduced during drone flights by improving the performance of hardware facilities. In fact, for a drone, it's not just hardware that matters, its core control system is also important. At present, several mainstream open source flight controls all use PID control algorithm to achieve the attitude and trajectory control of drones. The typical representative is PX4, whose software code system is relatively simple and clear. Therefore, based on the traditional PID control theory, a more adaptable UAV flight control system can not only reduce the probability of accidental crash during UAV flight to a certain extent, but also improve the control effect, reduce the hardware requirements of existing UAV, and provide a new way of thinking for low-cost civilian UAV [2-3].

In this paper, the motion model of the four-rotor drone aircraft control system is established by Newton-Eura method, and the control system is designed for attitude controller, low-cost combination navigation and four-rotor drone brushless DC motor. The original data of the attitude controller is processed by Kalman filtering to get the estimate of the current state, and the current position information of the drone is read by low-cost combined navigation. Based on the serial PID controller, a system design scheme with output of four brushless DC motor speed control is designed and is used in the actual system.

II. MATHEMATICAL MODEL OF QUADROTOR UAV

The dynamic model of the four-rotor unmanned aerial vehicle control system is established by Newton-Eura method, as shown in Fig. 2. In the two coordinate systems, the four-rotor drone is controlled by the rotation of the four rotary wings, in which the motors M1 and M3 rotate clockwise at the angle speed of s_1 and s_3 respectively, generating thrust f_1 and f_3 , respectively. At the same time, the other two motors (M2 and M4) rotate counterclockwise at the adverb velocity of s_2 and s_4 , generating thrust f_2 and f_4 , respectively.

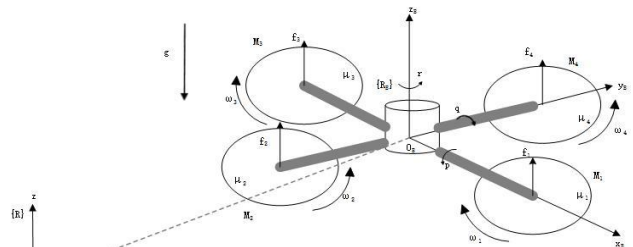


Fig. 1: Dynamic model of quadrotor UAV

In order to control the aircraft, it is necessary to define a spatial reference coordinate system and an ontology coordinate system fixed to the aircraft. The relative relationship between the two coordinate systems describes the motion state of the aircraft [4]. In Fig.1, $Oxyz$ is the Inertial coordinate system and $OBxByBzB$ is the Body frame. The origin of the body coordinate system is fixed to the mass of the drone [5].

$p_o^I = [x \ y \ z]^T$ is used to represent the position of the origin O_B of the Body frame in the inertial system, $v_o^I = [x \ y \ z]^T$ is used to represent the velocity vector of the drone at the inertial coordinates, and $v_o^B = [u \ v \ w]^T$ is used to represent the speed vector under the Body frame. The

three horns ϕ , θ , Ψ represent the direction of the Body system relative to the inertial coordinate system, and the angle velocity vector $\omega_B = [p \ q \ r]^T$ indicates the momentary adverb velocity of the axes of the ontology coordinate system. Among them, the rolling angle ϕ is the angle between the symmetrical plane of the drones and the lead vertical plane containing the shaft, the angle when rolling to the right is positive, the pitch angle θ is the angle between the body axis Ox_B and the horizontal Oxy plane, the head of the drone is positive, the deflection angle Ψ is the angle between the projection OxB and axis on the body axis Oxy and the horizontal OxB plane, and the angle of the drone when the right is deflected.

Vector v_o^B of the Body coordinate system is known, and vector v_o^I in the inertial coordinate system can be expressed as:

$$v_o^I = Rv_o^B \quad (1)$$

To find the conversion matrix R , the right-handed rules (in the order in which the $z \rightarrow x \rightarrow y$ rotates) are used. OX_1 , OY_1 , OZ_1 and OX_2 , OY_2 , OZ_2 are the transition axes at rotation, multiplied by the corresponding matrix generated by each rotation, and the transformation matrix R of the Body coordinate system to the inertial coordinate system is:

$$R = \begin{bmatrix} C_\theta C_\psi & C_\psi S_\theta S_\phi - C_\phi S_\psi & C_\theta C_\psi S_\theta + S_\phi S_\psi \\ C_\theta S_\psi & S_\theta S_\phi S_\psi + C_\phi C_\psi & C_\phi S_\theta S_\psi - C_\psi S_\phi \\ -S_\theta & C_\theta S_\phi & C_\theta C_\phi \end{bmatrix} \quad (2)$$

where $S(\cdot)$, $C(\cdot)$, and $T(\cdot)$ represent $\sin(\cdot)$, $\cos(\cdot)$ and $\tan(\cdot)$, respectively.

Since R is an orthogonal matrix, it is satisfied $R^{-1} = R^T$.

Thus, the positional motion equation writes the components in the form of:

$$\dot{x} = uC_\theta C_\psi + v(C_\psi S_\theta S_\phi - C_\phi S_\psi) + w(C_\theta C_\psi S_\theta + S_\phi S_\psi) \quad (3)$$

$$\dot{y} = uC_\theta S_\psi + v(S_\theta S_\phi S_\psi + C_\phi C_\psi) + w(C_\phi S_\theta S_\psi - C_\psi S_\phi) \quad (4)$$

$$\dot{z} = -uS_\theta + vS_\phi C_\theta + wC_\theta C_\phi \quad (5)$$

Similarly, the motion equation for Cape Eura is:

$$\begin{aligned} \dot{\phi} &= p + qS_\theta T_\theta + rC_\theta T_\theta \\ \dot{\theta} &= qC_\phi - rS_\phi \end{aligned} \quad (6)$$

$$\begin{aligned} \dot{\psi} &= \frac{1}{C_\theta} [qS_\phi + rC_\phi] \\ v_c^I &= Rv_c^B = R(v_o^B + \omega^B \times r_g^B) \end{aligned} \quad (7)$$

III. DESIGN OF CONTROL SYSTEM FOR QUADROTOR UAV

A. Mega2560

Arduino Mega 2560 is a micro control board based on ATmega2560. It has 54 digital input or output ports (15 of

which can be used as PWM output), 16 analog input ports, 4 UART serial ports, 16 MHz crystal oscillator, USB connection port, battery interface, ICSP head and reset button. This type of Arduino can just connect the computer with USB or a voltage transformer.

B. Hardware Design

The design uses the Arduino Mega2560 as the core control board, the MPU6050 sensor to control the stability of the UAV attitude, and the VL53L0X sensor to achieve the drone height [6]. By sensing the displacement changes of the aircraft on the X, Y and Z axes, each motor is controlled to compensate for the power to maintain the balance of the entire aircraft. The overall design of the hardware circuit is shown in Fig. 2.

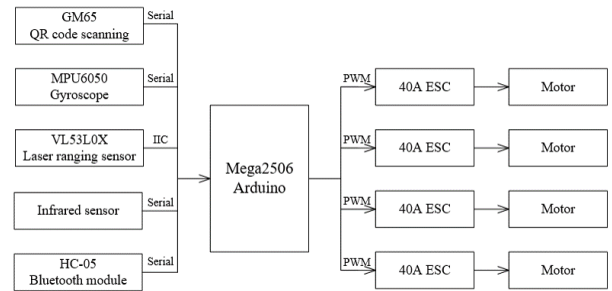


Fig. 2: Overall design scheme of hardware circuit

The gyroscope used in this design is mpu6050, which is an integrated 6-axis motion processing component. Compared with the multi-component scheme, it avoids the problem of the time axis difference between the combined gyroscope and accelerometer, and reduces a lot of packaging space.

In this design, the angle and angular velocity of UAV can be obtained by transmitting the information from gyroscope to MCU [7-8]. Therefore, in the design of hardware circuit, the output interface and level conversion device are designed to obtain information and provide energy to the gyroscope. The hardware circuit schematic design of gyroscope module is shown in Fig. 3.

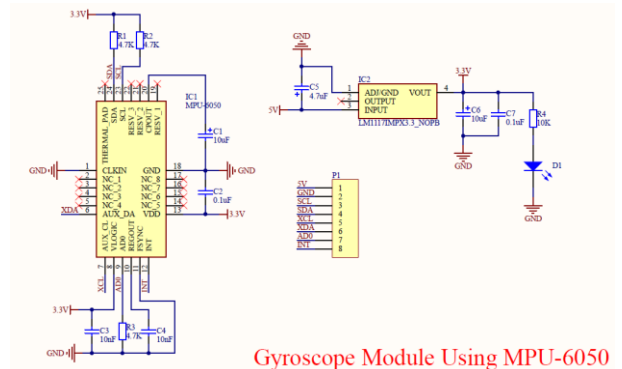


Fig. 3: Schematic design of Gyroscope module

ESC (Electronic speed control) module adjust the speed of the motor according to the control signal [9]. The EMC module in this design uses a mega8l MCU chip, two independent level conversion circuits, three-phase power inverter circuit and multi-point voltage detection [10]. It

takes 11.1V voltage as power supply input, and external MCU gives 5V control voltage and PWM control signal. The internal MCU peripheral circuit of EMC module is shown in Fig. 4.

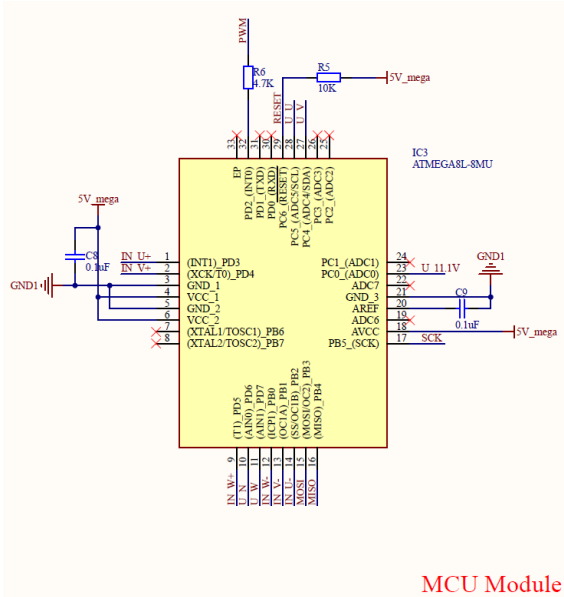


Fig. 4: Schematic design of MCU peripheral circuit in ESC module

The design scheme of the level conversion furnace is shown in Fig. 5. The energy source is an external battery, which is supplied through the plug.

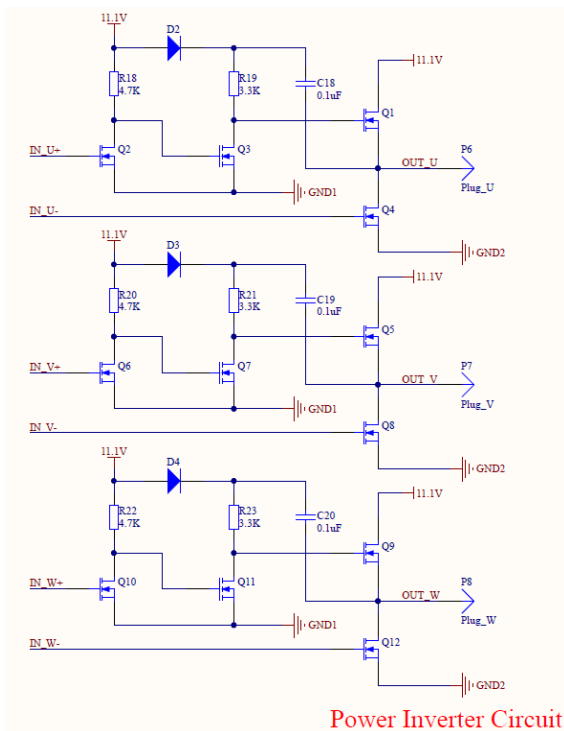


Fig. 5: Schematic design of power inverter in ESC module

In order to ensure the control of the circuit, it is necessary to detect the phase voltage, neutral point voltage and supply voltage in real time and send them to the internal MCU. Due to the large voltage, it is necessary to divide the voltage through the resistance to the MCU.

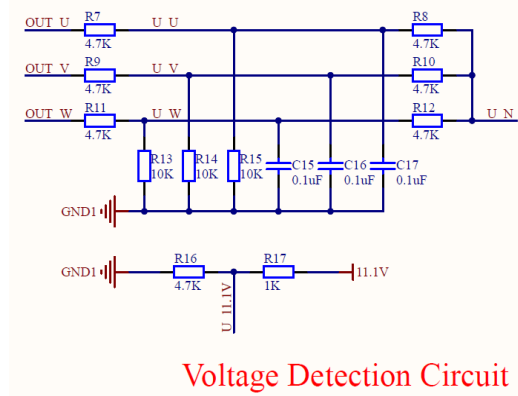


Fig. 6: Schematic design of voltage detection circuit in ESC module

The ESC module proposed above needs to use four groups in the design of the quadrotor UAV in this paper.

C. Software Design

In the program design, the serial PID type adaptive control is essentially two PIDs string together, divided into inner ring and outer ring PID [11]. Single-stage PID input is the actual angle, feedback is angle data, string-level PID foreign ring input feedback is also angle data, inner ring input feedback is aching velocity data. The executor can indirectly control the angle of the difference, that is, the adverb velocity, so as to achieve the goal of indirectly controlling the physical amount of the target, so that the four axes can still maintain the stability of the system when the attitude changes dramatically. The control block diagram is shown in Fig. 7.

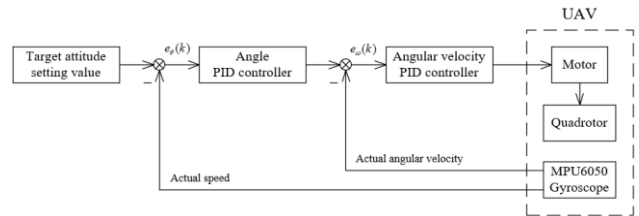


Fig. 7: Block diagram of cascade adaptive PID control system

The control logic and calculation method of outer loop PI and inner loop PID are given in Fig. 8.

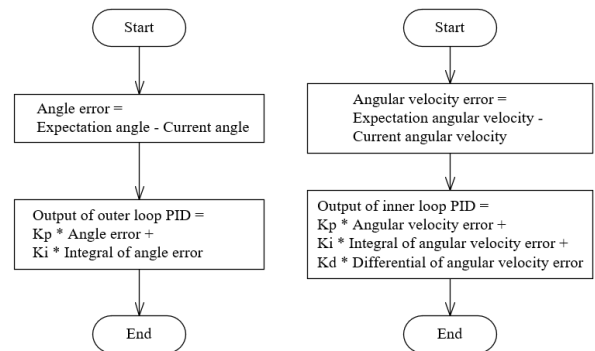


Fig. 8: Control logic diagram of outer loop PI and inner loop PID

IV. SIMULATION AND EXPERIMENTAL VALIDATION

A. Simulation Results

Based on MATLAB/Simulink, the simulation validation is carried out. The simulation result of the motor speed is shown in Fig. 9, showing that the reference speed can be effectively tracked.

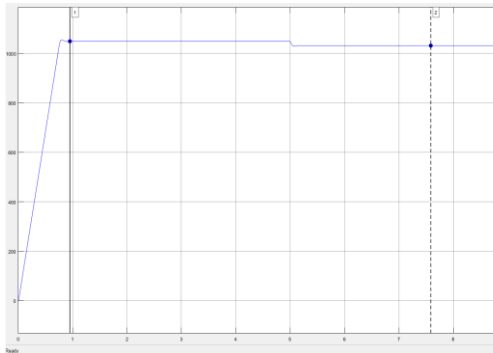


Fig. 9: Speed waveform

B. Experimental Results

Based on the designed scheme, this design is realized by 3D printing material structure and self-designed circuit system. This design uses a set of brackets, a control unit, a gyroscope, an infrared sensor, a ranging sensor, a two-dimensional code scanner, four electronic speed control, four motors and four propellers. The physical figure is shown in Fig. 10.

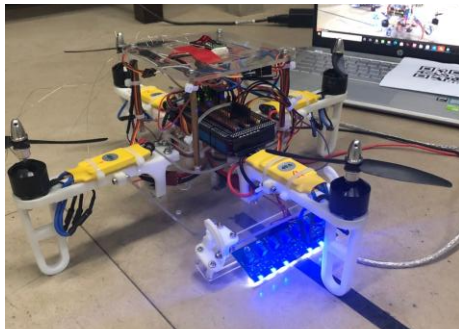


Fig.10. A picture of quadrotor UAV

Fig.11 shows the simulation result of the motor speed, showing that the reference speed can be effectively tracked even when the load is changed.

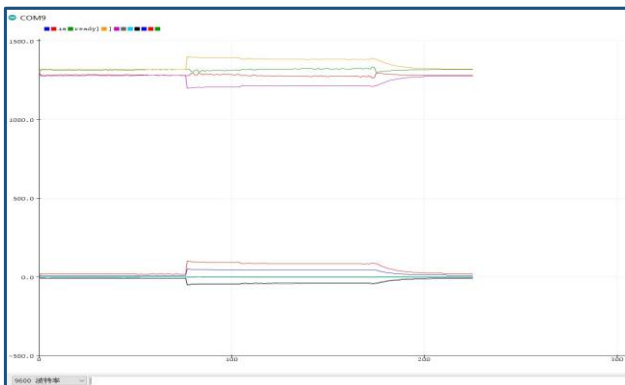


Fig. 11: Experimental waveform of speed.

V. CONCLUSION

The simulation and experiment results verified that the four rotor UAV proposed in this design has the anti-jamming and low-cost advantages. The circuit design applied in this design can not only be used in the example of quadrotor UAV, but also provide a reference scheme for other equipment which need to use gyroscope and electronic speed control.

REFERENCES

- [1] Tavooosi, J.: ‘Hybrid intelligent adaptive controller for tiltrotor UAV’, International Journal of Intelligent Unmanned Systems, 2020, advance online publication, doi:10.1108/ijius-05-2020-0009
- [2] Eugene L. and Kevin A.W.: ‘Robust and Adaptive Control With Aerospace Applications’ (Springer, 2013).
- [3] Ruan, Y.H., Zhang, Y., Li, Y.Z., Zhang, R. and Hang, RN.: ‘An Adaptive Channel Division MAC Protocol for High Dynamic UAV Networks’, IEEE Sensors Journal, 20, (11), 2020, pp. 9528-9539.
- [4] Noordin, A., Basri, MAM., Mohamed, Z. and Lazim, IM.: ‘Adaptive PID Controller Using Sliding Mode Control Approaches for Quadrotor UAV Attitude and Position Stabilization’, Arabian Journal for Science and Engineering, 2020, advance online publication, doi:10.1007/s13369-020-04742-w
- [5] Yang, S.Y., Han, J., Xia, L. and Chen, Y.H.: ‘Adaptive robust servo constraint tracking control for an underactuated quadrotor UAV with mismatched uncertainties’, ISA transactions, 106, 2020, pp. 12-30.
- [6] Aleksander N. and Zygmunt K.: ‘Vision Based Systems for UAV Applications’ (Springer, 2013).
- [7] Liu, W.H. and Dai, J.X.: ‘Design of Attitude Sensor Acquisition System Based On STM32’, Proceedings of 5th International Conference on Instrumentation & Measurement, Computer, Communication, and Control (IMCCC), 2015, pp. 1850-1853.
- [8] Huang, J.: ‘Design of Angle Detection System Based on MPU6050’, Proceedings of 7th International Conference on Education, Management, Information and Computer Science (ICEMC), 73, 2017, pp. 6-8.
- [9] Wang, J.Y.: ‘Design of small power servo brushless DC motor driver’, Advanced Materials Research, 694-697, 2013, pp. 1569-1572.
- [10] Gao, X.Z., Zhang, P. and Wang, W.: ‘A simple, superior, practical design of brushless DC motor system’, Advanced Materials Research, 846-847, 2014, pp. 65-68.
- [11] Zhao, X.Y., Chen, Z.W. and Zhou, Y.H.: ‘Realization of H-Bridge DC Motor Drive Based on AVR Singlechip’, Proceedings of 9th International Symposium on Test and Measurement (ISTM), 2011, pp. 39-42.

Topology and Analysis of An Electromechanical Brake for Electric Vehicles

Xiangdang XUE, Ka Wai Eric CHENG, and Yulong FAN

Power Electronics Research Centre, Department of Electrical Engineering, The Hong Kong Polytechnic University, Hong Kong, China
E-mail: xd.xue@polyu.edu.hk, eecheng@polyu.edu.hk

Abstract– A new automotive electromechanical brake (EMB) is proposed in this study, which consists of the electromagnetic linear actuator that includes the stator and the mover, the power rod, the wedge, the braking pads, the caliper and the mechanical accessory. The braking torque is controlled via the actuator control unit. The topology structure of the proposed EMB is discussed. The models of the proposed EMB are developed, it is confirmed that the proposed EMB provides two braking forces with same magnitude and opposite direction to the braking pads, and the gains of the components and the proposed EMB are formulated. Furthermore, the effects of the geometrical parameter and the design parameter on the performance of the proposed EMB are analyzed via simulation. This study provides a novel EMB topology for electric vehicles, which possesses the faster dynamic response than previous EMBs.

Keywords–Braking system, electric vehicles (EV), electromechanical brake (EMB).

I. INTRODUCTION

For current commercial automobiles, hydraulic or electrohydraulic wheel brakes are used popularly. However, those brakes possess the inherent disadvantages, such as the flammable braking fluid, the leakage of the braking fluid and the discontinuous control of the braking torque, which degraded automotive safety, ABS performance and environmental protection. An alternative solution is being concerned, which is the electromechanical brake (EMB) [1]-[5]. Without any hydraulic component, the electromechanical brakes are controlled electrically. The electromechanical brakes have a number of potential advantages compared with conventional electrohydraulic brakes, such as faster dynamic response, more accurate braking torque control, continuous control of braking torque, improved braking and stability behavior, no flammable fluids, and reduction in complexity and quantity of components. Thus, the electromechanical brakes are regarded as the next generation of automotive wheel brakes.

II. TOPOLOGY OF PROPOSED ELECTROMECHANICAL BRAKE

Fig. 1 illustrates the topology of the proposed electromechanical brake. It consists of the electromagnetic linear actuator that includes the stator and the mover, the power rod, the wedge, the braking pads, the caliper and the accessory.

The operation of the proposed electromechanical brake can be summarized as follows. The electromagnetic linear actuator is controlled by its control unit, in which the input voltage signal is used to control the electromagnetic force

output by the mover. The electromagnetic force is appropriately proportional to the input voltage signal. Via the mechanical link between the mover and the right terminal of the power rod, the electromagnetic force is transferred to the right terminal of the power rod. Due to the mechanism of the power pod, the force applied to the right terminal of the power rod is transferred to the left terminal of the power pod. Via the mechanical link between the left terminal of the power rod and the wedge, the force applied to the left terminal of the power rod is transferred to the wedge. Consequently, the force applied to the wedge makes the wedge move up or down. The up motion of the wedge further results in that the right braking pad moves left, and the caliper moves right. Moreover, the right motion of the caliper makes the left braking pad moves right. Thereby, two braking pads move toward the braking disc, until two braking pads contact the braking disc to generate the braking torque applied to the braking disc. The electromagnetic force is zero and the wedge and two braking pads release if the input voltage signal is zero.

The effect diagram that the proposed electromechanical brake is applied to the automotive wheel is shown in Fig. 2.

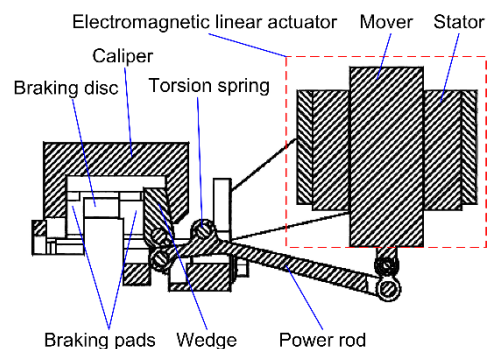


Fig. 1 Topology of proposed electromechanical brake

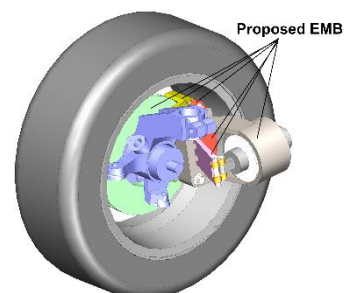


Fig. 2 Integration between wheel and proposed electromechanical brake

The electromechanical brake unit consists of the electromechanical brake and the actuator control unit. The schematic structure of the electromechanical brake unit is illustrated in Fig. 3.

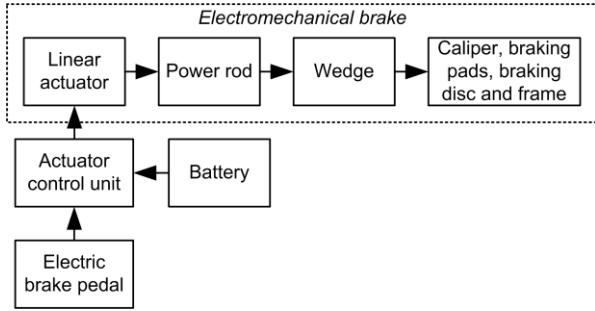


Fig. 3 Control schematic of proposed electromechanical brake

III. MODELS OF PROPOSED ELECTROMECHANICAL BRAKE

1. Model of Electromagnetic Linear Actuator

The model of the electromagnetic linear actuator is illustrated in Fig. 4, in which the input voltage signal (V_{in}) is converted into the electromagnetic force (F_{em}) by the electromagnetic linear actuator and the conversion coefficient is K_c . It is assumed that the electromagnetic linear actuator generates the down electromagnetic force in the subsequent analysis, in which the gravities of all the components are neglected.

Referring to Fig. 4, the relationship between the electromagnetic force output by the mover and the voltage signal input to the control unit of the electromagnetic linear actuator can be expressed as

$$F_{em} = K_c V_{in} \quad (1)$$

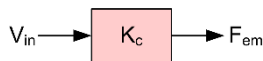


Fig. 4 Model of electromagnetic linear actuator

2. Model of Power Rod

Fig. 5 illustrates the model of the power rod, in which F_{rt} represents the force applied to the right terminal of the power rod, L_r the length of the right arm of the power rod, F_{lt} the force applied to the left terminal of the power rod, and L_l the length of the left arm of the power rod.

The force (F_{rt}) applied to the right terminal of the power rod is equal to the electromagnetic force (F_{em}) if the loss of

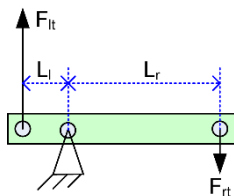


Fig. 5 Model of power rod
International Conference on Power Electronics Systems and Applications (PESA 2020)

the mechanical link is ignored. Thus, one has

$$F_{rt} = F_{em} \quad (2)$$

At the same time, the force applied to the left terminal of the power rod can be calculated as

$$F_{lt} = \frac{L_r}{L_l} F_{rt} \quad (3)$$

3. Model of Wedge

The model of the wedge is illustrated in Fig. 6 when the wedge and the caliper are at standstill. In Fig. 6, α represents the wedge angle, F_{rw} the force applied to the wedge by the left terminal of the power rod, F_{pw} the normal force applied to the wedge by the right braking pad, F_{cw} the normal force applied to the wedge by the caliper, F_{fpw} the friction force between the right braking pad and the left wedge surface, and F_{fcw} the friction force between the caliper slope surface and the wedge slope surface.

The force balance equation in the horizontal direction can

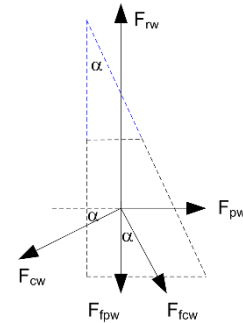


Fig. 6 Model of wedge

be expressed as

$$F_{cw} \cos \alpha = F_{pw} + F_{fcw} \sin \alpha \quad (4)$$

The force balance equation in the vertical direction can be given as

$$F_{rw} = F_{cw} \sin \alpha + F_{fpw} + F_{fcw} \cos \alpha \quad (5)$$

where F_{rw} is equal to F_{lt} .

The friction force between the right braking pad and the wedge can be calculated as

$$F_{fpw} = \mu_f F_{pw} \quad (6)$$

where μ_f is the friction coefficient.

The friction force between the caliper and the wedge can be calculated as

$$F_{fcw} = \mu_f F_{cw} \quad (7)$$

4. Model of Caliper

The model of the caliper is shown in Fig. 7 when the wedge and the caliper are at standstill. In Fig. 7, F_{wc} represents the normal force applied to the caliper by the wedge, F_{pc} the normal force applied to the caliper by the left braking pad, F_{fwc} the friction force between the wedge slope surface and the caliper slope surface, and F_{sc} the force applied to the caliper by the support.

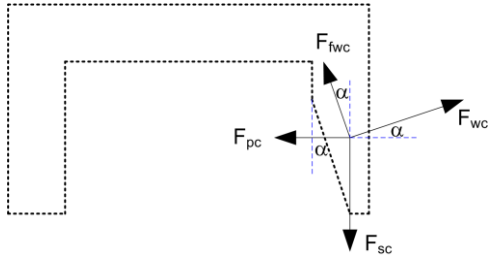


Fig. 7 Model of caliper

The force balance equation in the horizontal direction can be expressed as

$$F_{wc} \cos \alpha = F_{pc} + F_{fwc} \sin \alpha \quad (8)$$

The force balance equation in the vertical direction can be given as

$$F_{sc} = F_{wc} \sin \alpha + F_{fwc} \cos \alpha \quad (9)$$

Furthermore, one has

$$F_{fwc} = F_{fcw} \quad (10)$$

$$F_{wc} = F_{cw} \quad (11)$$

$$F_{wp} = F_{pw} \quad (12)$$

$$F_{cp} = F_{pc} \quad (13)$$

where F_{cp} represents the normal force applied to the left braking pad by the caliper.

5. Braking Force Applied to Two Braking Pads

From the equations (4) (7), the normal force applied to the wedge by the right braking pad can be calculated as

$$F_{pw} = F_{cw} - \mu_f F_{cw} \sin \alpha \quad (14)$$

From the equations (8) (10) (11), the normal force applied to caliper by the left braking pad can be expressed as

$$F_{pc} = F_{cw} - \mu_f F_{cw} \sin \alpha \quad (15)$$

Referring to the equations (12)-(15), it can be seen that the normal force applied to the right braking pad is equal to the normal force applied to the left braking pad. In other words, thus, the braking force applied to the right braking pad and the braking force applied to the left braking pad have the same magnitude and the opposite direction. It meets the requirement of the wheel brakes.

6. Vertical Displacement of Wedge and Horizontal Displacement of Braking Pads

The wedge only moves vertically in the proposed electromechanical brake. Due to the wedge's structure, however, the wedge is capable of generating the horizontal displacement if the wedge moves vertically to result in the vertical displacement. The relationship between the vertical wedge displacement and the horizontal wedge displacement is shown in Fig. 8, if the wedge moves upward.

If the vertical wedge displacement is D_y , referring to Fig. 8, the horizontal wedge displacement (D_x) can be calculated as

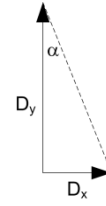


Fig. 8 Vertical and horizontal displacements of wedge

$$D_x = D_y \tan \alpha \quad (16)$$

The horizontal displacement generated by the wedge results in that two braking pads move toward the braking disc. Consequently, the relationship between the horizontal wedge displacement and the horizontal displacement of the braking pad (D_p) can be expressed as

$$D_x = 2D_p \quad (17)$$

Thereby, the relationship between the vertical wedge displacement and the horizontal displacement of the braking pad can be expressed as

$$D_y = \frac{2D_p}{\tan \alpha} \quad (18)$$

7. Gains of Proposed Electromechanical Brake

Table I shows the gains of three components and the proposed electromechanical brake. The gain of the electromagnetic linear actuator (G_a) is defined as the ratio of the electromagnetic force to the input voltage signal, the gain of the power rod (G_r) is defined as the ratio of the force applied to the left rod terminal to the force applied to the right rod terminal, the gain of the wedge (G_w) is defined as the ratio of the force applied to the right braking pad by the wedge and the force applied to the wedge by the left rod terminal, and the gain of the electromechanical brake (G_{EMB}) is defined as the ratio of the force applied to the right braking pad by the wedge to the input voltage signal. These gains can be obtained from the equations (1)-(15).

Table 1: Gains of proposed electromechanical brake

Gain	Value
G_a	K_c
G_r	L_r/L_l
G_w	$\frac{\cos \alpha - \mu_f \sin \alpha}{\sin \alpha + 2\mu_f \cos \alpha - \mu_f^2 \sin \alpha}$
G_{EMB}	$\frac{K_c L_r (\cos \alpha - \mu_f \sin \alpha)}{L_l (\sin \alpha + 2\mu_f \cos \alpha - \mu_f^2 \sin \alpha)}$

IV. ANALYSIS OF PROPOSED ELECTROMAGNETIC BRAKE

1. Effect of Wedge Angle on Gain of Wedge

For the proposed electromechanical brake, it can be seen from Table I that the gain of the wedge depends on the

wedge angle and the friction coefficient. The effect of the wedge angle on the wedge's gain is illustrated in Fig. 9 if the friction coefficient is equal to 0.1. It can be observed from Fig. 9 that the gain of the wedge decreases for the specified friction coefficient if the wedge angle becomes large. Consequently, the wedge angle should be designed as the small angle, to obtain the high gain of the wedge.

2. Effect of Friction Coefficient on Gain of Wedge

Fig. 10 illustrates the effect of the friction coefficient on the wedge's gain if the wedge angle is 15 degree. It can be observed from Fig. 10 that the gain of the wedge decreases for the specified wedge angle if the friction coefficient between the wedge surfaces and the other surfaces becomes high. Thereby, the friction coefficient should be selected as the low value, to obtain the high gain of the wedge.

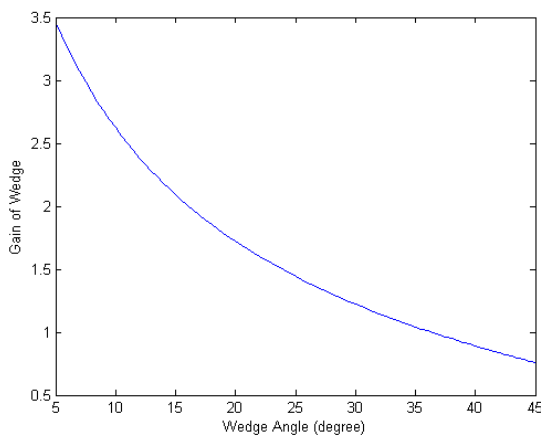


Fig. 9 Effect of wedge angle on wedge's gain

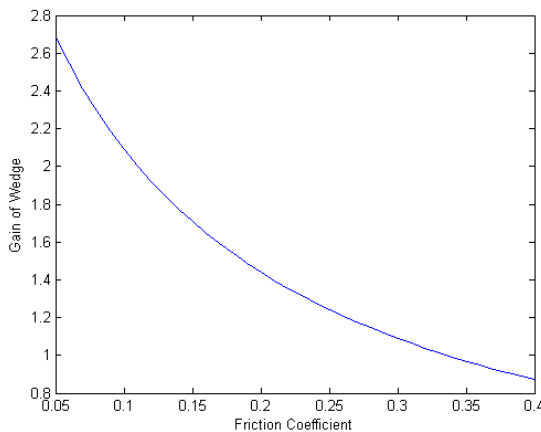


Fig. 10 Effect of friction coefficient on wedge's gain

3. Effect of Wedge Angle on Maximum Displacement of Braking Pad

The effect of the wedge angle on the maximum displacement of the braking pad is shown in Fig. 11 if the maximum vertical displacement of the wedge is 10 mm. It can be seen from Fig. 11 that the maximum displacement

of the braking pad increases for the specified maximum vertical displacement of the wedge if the wedge angle becomes large. Therefore, the wedge angle should be designed appropriately, to guarantee that the maximum displacement of the braking pad is more than the clearance of the braking pad, which is the distance between the braking disc and the braking pad at the releasing position of the braking pads.

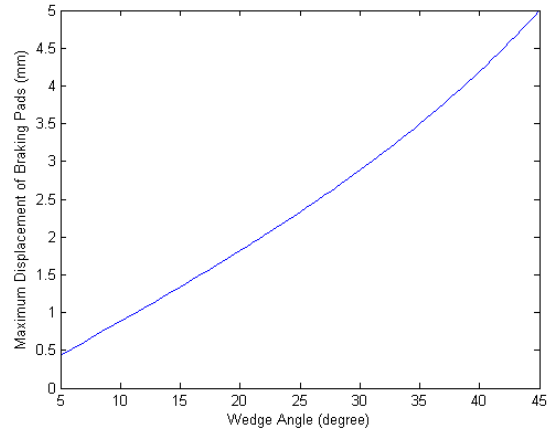


Fig. 11 Effect of wedge angle on maximum displacement of braking pads

V. CONCLUSION

The electromechanical brake with the new topology and behavior has been proposed in this paper, which is applicable to wheel brakes in electric vehicles and controlled electrically without any hydraulic component. The models of the components in the proposed electromechanical brake have been developed, which can be used to complete the design of the proposed electromechanical brake. The theoretical analysis has confirmed that the braking force applied to the right braking pad and the braking force applied to the left braking pad have the same magnitude and the opposite direction. The simulation analysis shows that the wedge angle has the considerable effects on the gain of the wedge and the maximum displacement of the braking pads for the specified maximum vertical displacement of the wedge, and the friction coefficient between the wedge surfaces and the surfaces of other components has the significant effect on the gain of the wedge. The wedge angle should be selected appropriately, to obtain the sufficiently high gain of the wedge and the enough large displacement of the braking pads. The friction coefficient should be designed as low as possible, to obtain the high gain of the wedge.

ACKNOWLEDGMENT

The authors would like to thank the part financial support from the Guangdong-Hong Kong Technology Cooperation Funding Scheme of Hong Kong Innovation and Technology Support Programme under Grant GHP/033/17AP.

REFERENCES

- [1] Reza Hoseinnezhad, Alireza Bab-Hadiashar, and Tony Rocco, "Real-Time Clamp Force Measurement in Electromechanical Brake Calipers", IEEE TRANSACTIONS ON VEHICULAR TECHNOLOGY, VOL. 57, NO. 2, MARCH 2008, pp. 770-777, DOI 10.1109/TVT.2007.906374.
- [2] Chihoon Jo, Sungho Hwang, and Hyunsoo Kim, "Clamping-Force Control for Electromechanical Brake", IEEE TRANSACTIONS ON VEHICULAR TECHNOLOGY, VOL. 59, NO. 7, SEPTEMBER 2010, pp. 3205-3212 DOI 10.1109/TVT.2010.2043696.
- [3] Jiweon Ko, Sungyeon Ko, Hanho Son, Byoungsoo Yoo, Jaeseung Cheon, and Hyunsoo Kim, "Development of Brake System and Regenerative Braking Cooperative Control Algorithm for Automatic-Transmission-Based Hybrid Electric Vehicles", IEEE TRANSACTIONS ON VEHICULAR TECHNOLOGY, VOL. 64, NO. 2, FEBRUARY 2015, pp. 431-440, DOI 10.1109/TVT.2014.2325056.
- [4] Heeram Park and Seibum B. Choi, "Development of a Sensorless Control Method for a Self-Energizing Brake System Using Noncircular Gears", IEEE TRANSACTIONS ON CONTROL SYSTEMS TECHNOLOGY, VOL. 21, NO. 4, JULY 2013, pp. 1328-1339, DOI 10.1109/TCST.2012.2204750.
- [5] Sangjune Eum, Jihun Choi, Sang-Shin Park, Changhee Yoo and Kanghyun Nam, "Robust Clamping Force Control of an Electro-Mechanical Brake System for Application to Commercial City Buses", Energies 2017, 10, 220, pp. 1-12, DOI 10.3390/en10020220.

Research on Symmetry Half-Bridge Switched Capacitor Active Equalization Circuit of Vehicle Power Lead-Acid Battery

Mingyu Gao¹, Jifeng Qu¹, Junfan Wang¹, Huipin Lin¹, Minghao Wang²

¹School of Electronics and Information, Hangzhou Dianzi University, Hangzhou, P. R. China

²Department of Electrical Engineering, The Hong Kong Polytechnic University, Hong Kong

E-mail: {mackgao, qujifeng, wangjunfan, linhuipin}@hdu.edu.cn¹

Abstract –In view of the complex battery equalization control in the traditional active equalization strategy of lead-acid batteries. In the traditional lead-acid battery active equalization strategy, the isolated drive circuit of the power switch is complicated and its stability is poor. A new equalization strategy based on half-bridge switch structure, moderate cost, easy to control, and high stability is proposed. The proposed scheme is suitable for equalization applications with a small number of battery cells, and the battery capacity is large, similar to lead acid battery. The proposed scheme is simulated and verified by Simetrix-Simplis 8.20, and the working conditions of the power battery in vehicles are analyzed and demonstrated, and the complete control strategies are developed for various working scenarios, and they are verified by experiment. The experimental results demonstrate that the proposed equalization scheme can accomplish the equalization work continuously, stably and efficiently.

Keywords – Lead-Acid battery equalization, Symmetry half-bridge driver, Switched capacitor

I. INTRODUCTION

Lead-acid batteries are still widely used in low-end areas of power batteries [1], which have a high cost-effective ratio compared to lithium batteries, and they have no memory effect as lithium batteries. The lead-acid battery cell rated voltage is 12V and requires multiple lead-acid battery cells in series to meet the needs of different applications in practice [2]. Similar to other types of batteries, lead-acid cells can be skewed in the manufacturing process, although factory-specific battery cells are distributed in a group through schemes such as battery packing, the differences between cells are inevitable. As usage time increases, similar batteries can be in different states due to complex usage. As the degree of imbalance increases, directly back to the lead-acid battery pack where individual batteries cannot be fully charged due to the "barrel effect" [3]. Lead-acid batteries over discharge or overcharge for a long time will eventually lead to the battery plate vulcanization [4]. Vulcanization is the main factor to reduce the capacity and

shorten the life of lead-acid battery. To extend battery life, imbalances must be suppressed as much as possible over the life period of the battery [5]. An effective way to reduce imbalances is equalization. The passive equalization method narrows the difference between the cells by dissipation of energy [6]. For large-capacity lead-acid battery cells, it is unreasonable to achieve equalization by passive equalization because it wastes a lot of energy and generates a lot of heat. This method is not appropriate from an efficiency and security perspective [7]. Active equalization is also known as energy transfer equalization. The method is to transfer the unbalanced energy in some way until the balanced state is reached [8]. According to the critical devices used in active equalization to classify, active equalization mainly includes: inductive equalization, capacitive equalization, bidirectional Buck-Boost topology equalization, bidirectional flyback topology equalization [9], resonant equalization [10], etc. Capacitive equalization is more flexible than inductive equalization, and circuit topology has more research value [11]. In this paper, the method of active equalization of symmetric half-bridge switching capacitors is proposed, and a simple and reliable driving method is proposed for the key problem of switch isolation drive. The feasibility of the method is proved through theoretical analysis, simulation and actual circuit test.

II. TECHNICAL INFORMATION

A. Equalization system block diagram

As shown in Fig. 1, the system is divided into two parts: the control circuit and the equalization circuit. The control circuit collects the battery voltage data through the ADC channel and outputs PWM waveform for control. This part provides the consumer with a control interface and status indication. The equalization circuit consists of a symmetrical half-bridge switch array, a switch array drive circuit and a equalization capacitor array.

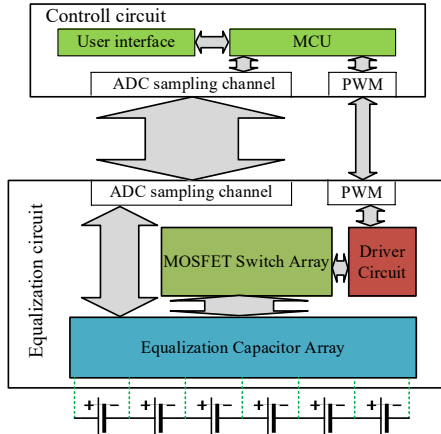


Fig. 1: equalization system block diagram

B. Symmetry half-bridge switch circuit and drive circuit

In this paper, a half-bridge switch structure is proposed to realize the function of capacitive charge and discharge circuit switching, and the local circuit structure diagram is

shown in Fig. 2. Take the B5 and B6 battery cells in Fig. 1 as an example.

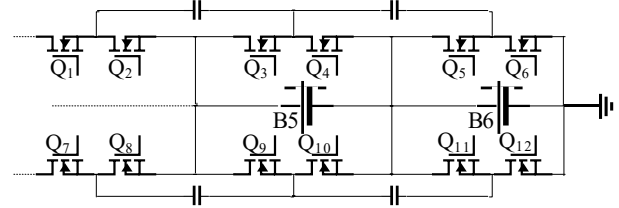


Fig. 2: Symmetry half-bridge switch circuit

The common drive circuit of the half-bridge structure only needs to float the upper half-bridge switch, but the float drive between each set of half-bridges in this particular structure of the battery pack is also a key point in the design. The float drive of the switch between the battery packs is also difficult. In this paper, a simple structure and moderate cost drive circuit are proposed for the complexity and high cost of traditional methods, the circuit structure is shown in Fig. 3, the corresponding control signal is shown in Fig. 4.

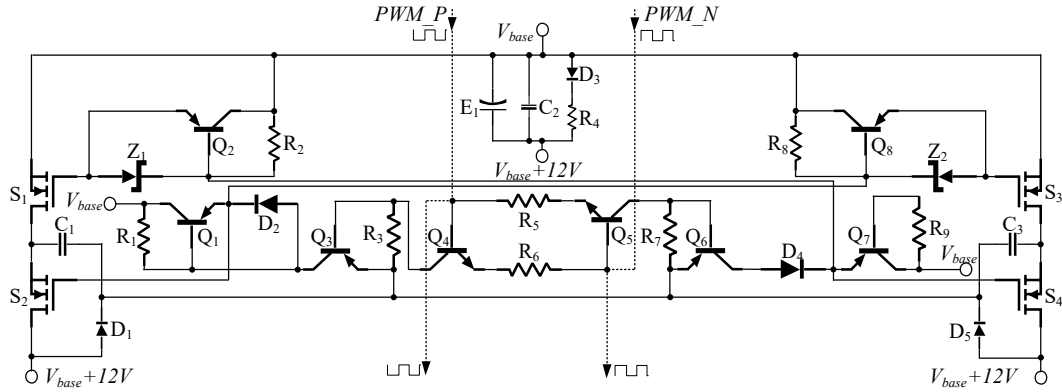


Fig. 3: Float half-bridge drive circuit

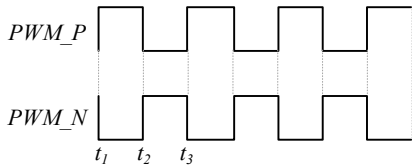


Fig. 4: Half-bridge drive circuit control signal

C. Equalization circuit parameter calculation

The method proposed in this paper is based on the traditional single-layer switched capacitor equalization topology. The theoretical analysis needs to pay attention to the process of voltage and current change during capacitor charging and the process of voltage change during capacitor discharge.

• Capacitor charging process

Ignore the loss caused by parasitic resistances such as transmission wires and switching devices, firstly analyze and calculate the charging process of the capacitor in the zero initial state. Assume that battery B5 in Fig. 5 is the source battery with a higher energy level, and B6 is the target battery with lower energy level.

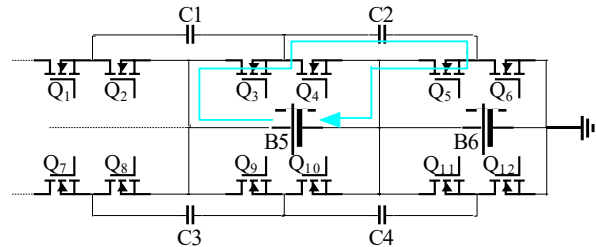


Fig. 5: Capacitor charging loop

The on resistance of single mosfet switch is R_{dson} , and the internal resistance of the battery is R . The discharge current of battery B5 passes through the two mosfet switches Q_4 and Q_5 . In this case, the equivalent circuit model of the charging loop is shown in Fig. 6.

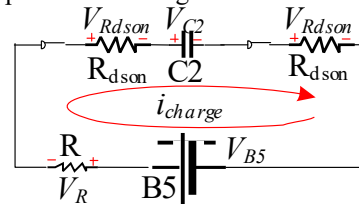


Fig. 6: Capacitor charging equivalent circuit

Because the charge and discharge are switched quickly, the battery voltage can be regarded as constant for a short time, equation (1) is obtained according to Kirchhoff's law.

$$V_{B5} = V_{C2} + 2V_{R_{dson}} + V_R \quad (1)$$

The voltage on the equivalent resistance is calculated according to equation (2). The charging current value i_{charge} is calculated according to equation(3).

$$2V_{R_{dson}} + V_R = i_{charge} (2R_{dson} + R) \quad (2)$$

$$i_{charge} = C \frac{dV_{C2}}{dt} \quad (3)$$

Combine equation (2) and equation(3) to get equation (4), which is a first-order linear differential equation with constant coefficients.

$$V_{B5} = V_{C2} + C(2R_{dson} + R) \frac{dV_{C2}}{dt} \quad (4)$$

The differential equation solving result is shown in equation (5),

$$-\ln(V_{B5} - V_{C2}) = \frac{t}{C(2R_{dson} + R)} + k \quad (5)$$

In equation (5), k is an arbitrary constant. Substitute boundary conditions $t=0, V_{C2}=0$, find $k = -\ln V_{B5}$, Substitute k into the last equation of equation (5), the capacitor voltage expression is obtained as shown in equation (6).

$$V_{C2} = V_{B5} - V_{B5} e^{-\frac{t}{C(2R_{dson} + R)}} \quad (6)$$

Then the change of the capacitor voltage with time is shown in Fig. 7.

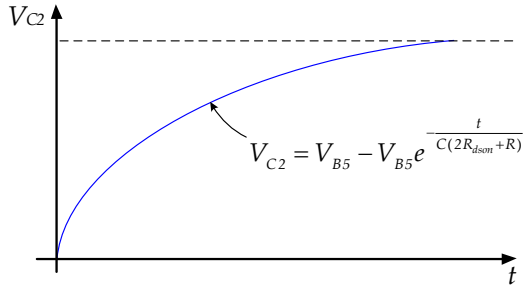


Fig. 7: Voltage curve of capacitor charging in zero state

Substitute the capacitor voltage into equation (3) to solve the loop current, the process is shown in equation (7),

$$V_{R_{total}} = V_{B5} - V_{C2} = V_{B5} e^{-\frac{t}{C(2R_{dson} + R)}} \quad (7)$$

$$i_{charge} = C \frac{dV_{C2}}{dt} = \frac{V_{B5}}{2R_{dson} + R} e^{-\frac{t}{C(2R_{dson} + R)}}$$

The current decay curve is shown in Fig.8,

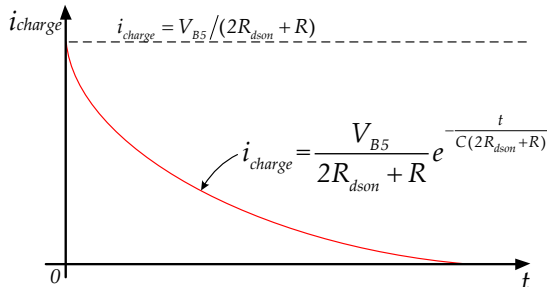


Fig. 8: Current decay curve of capacitor charging loop

The maximum current value that can be reached during the charging of the capacitor is $i_{charge} = V_{B5} / (2R_{dson} + R)$. The capacitance value of the capacitor needs to be estimated

based on the capacitor charging time constant and the selected switching frequency. The capacitor charging time constant is $\tau = C(2R_{dson} + R)$, ignoring the ESR of the capacitor. According to the selected on-resistance of the mosfet and the internal resistance of the lead-acid battery, the approximate capacitor charging time can be estimated. If the switching period is satisfied, the charging and discharging time requirement of the capacitor can be met.

- *Capacitor discharge process*

The process of capacitor C2 charging battery B6 is similar to the process mentioned above, the discharge equivalent circuit is shown in Fig. 9.

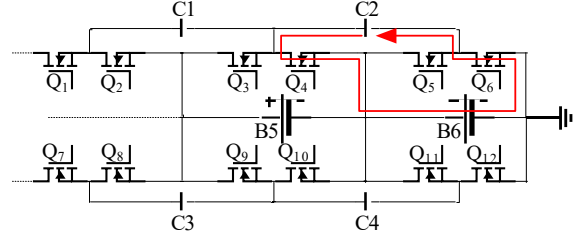


Fig. 9: Capacitor discharging loop

The capacitor will continue to discharge until the capacitor voltage is equal to the battery voltage. Suppose the voltage of battery B6 is V_{B6} . The equivalent circuit diagram of the discharge circuit is shown in Fig. 10.

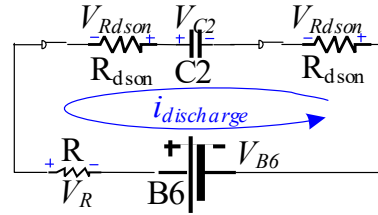


Fig. 10: Equivalent circuit of capacitor discharge

According to Kirchoff's law, list the equation as shown in equation (8). The voltage symbols used are redefined here,

$$V_{C2} = -2V_{R_{dson}} - V_R + V_{B6} \quad (8)$$

The capacitor discharge current is calculated according to equation (9),

$$2V_{R_{dson}} + V_R = i_{discharge} (2R_{dson} + R) \quad (9)$$

$$i_{discharge} = C \frac{d(V_{C2} - V_{B6})}{dt}$$

Write the differential equation as shown in equation (10),

$$V_{C2} = V_{B6} + C(2R_{dson} + R) \frac{d(V_{C2} - V_{B6})}{dt} \quad (10)$$

The process of solving this differential equation is similar to the process mentioned above, and equation (11) is obtained,

$$-\ln(V_{C2} - V_{B6}) = \frac{t}{C(2R_{dson} + R)} + k \quad (11)$$

k is an arbitrary constant, and the boundary condition $t=0, V_{C2}=V_{B5}$, find $k = -\ln(V_{B5} - V_{B6})$. Substituting k into equation (11) and solving, the capacitor voltage expression is obtained as shown in equation (12).

$$V_{C2} = V_{B6} + (V_{B5} - V_{B6}) e^{-\frac{t}{C(2R_{dson} + R)}} \quad (12)$$

The voltage change curve of the capacitor is shown in Fig.11.

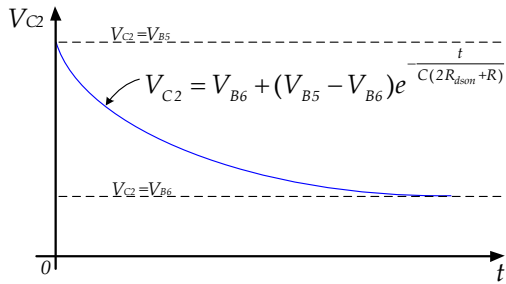


Fig. 11: Capacitor discharge voltage curve

The final capacitor voltage is equal to the battery voltage. The capacitor discharge current does not need to be concerned, only the maximum current peak value during the charging process needs to be estimated.

III. IMPLEMENTATION AND EXPERIMENTAL RESULTS

A. Experimental Parameters

The lead-acid batteries used in the experiment and the types and parameters of the devices are shown in Table 1.

Table 1: Devices and parameters

Item	Name	Parameters
Battery	6-DZF-12.2	12V 12.2Ah
Mosfet	VBE1307	$R_{dson}=10m\Omega$
Capacitor	16SEPC270MX	16V 270uf
Controller	STM32F030C8T6	-
Switching Freq.	-	16kHz

A total of 6 batteries were used in the experiment, and the maximum instantaneous peak current that the mosfet used as a switch can withstand is 250A.

B. Control Algorithm

Equalization algorithm is the key factor for efficient work of equalization system, most of the traditional algorithms are equalization algorithms for static battery systems, the equalization of the battery pack in actual use is not taken into account. For example, the status of vehicle start, vehicle stop and battery charging encountered in actual use of the power battery, this paper presents a dynamic equalization algorithm that include the operating status of the vehicle. The control algorithm is shown in Fig. 12.

The proposed equalization algorithm includes the starting and stopping of the vehicle, and the state of charging when the battery charging, which is closer to the actual working condition of the power battery equalization system.

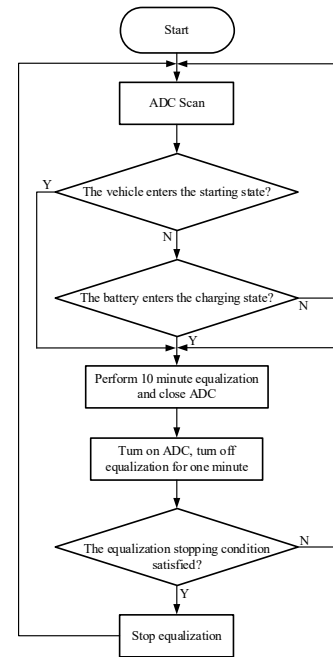


Fig. 12: Equalization strategy flowchart

C. Prototype of equalization circuit

The prototype and test equipment of the equalization system are shown in Fig. 13.

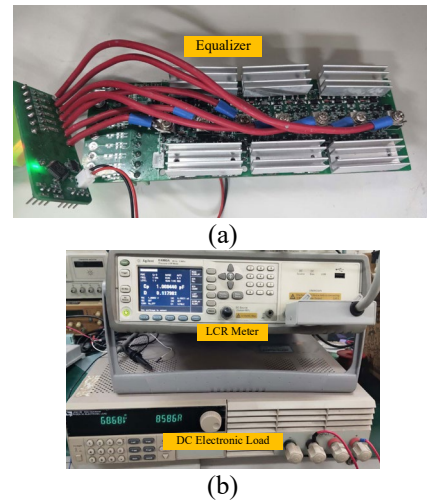


Fig. 13: Prototype and test equipment, (a) symmetrical half-bridge equalization board (b) LCR meter and electronic load.

In the experiment, six unbalanced 12V-12.2Ah lead-acid batteries were balanced. Artificially used chargers and electronic loads to create the required unbalanced state. The open circuit voltage state of the battery cell before equalization is shown in Table 2.

Table 2: Cell voltage before equalization

Cell number	Voltage
Cell1	13.824V
Cell2	12.928V
Cell3	12.514V
Cell4	11.514V
Cell5	11.092V
Cell6	10.768V

The signal waveforms of PWM_P and PWM_N in Fig. 3

are shown in Fig. 15.

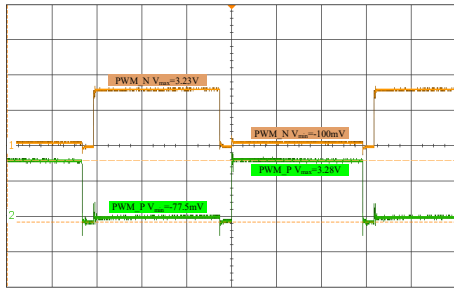


Fig. 15: Half-bridge drive circuit control signal

During the process, the relevant waveform of switch S4 in Fig. 3 is shown in Fig. 16.

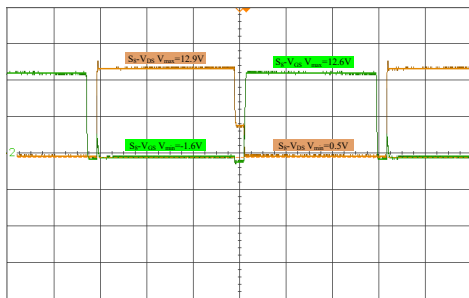


Fig. 16: GS and DS waveforms corresponding to switch S4 in Fig. 3

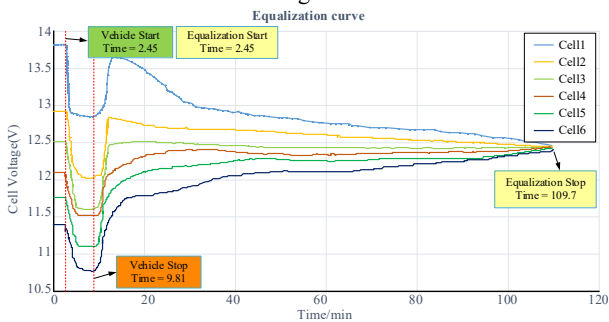


Fig. 17: Equalization curve

Table 3: Cell voltage after equalization

Cell number	Voltage
Cell1	12.463V
Cell2	12.449V
Cell3	12.439V
Cell4	12.441V
Cell5	12.425V
Cell6	12.414V

As shown in Fig. 17, the equalization circuit did not start before the vehicle started. The equalization circuit starts at Time = 2.45, and the vehicle stops at Time = 9.81. The equalization lasted for about 109.7 minutes and then stopped, after the equalization completed, the battery cell voltage is shown in Table 3.

IV. CONCLUSION

This paper proposes a symmetrical half-bridge switched capacitor balancing circuit topology. Aiming at the problem of floating drive of traditional battery pack power switch, the paper proposes a simple, reliable and easy-to-control half-bridge drive circuit. The equalization circuit proposed in the paper is suitable for the equalization of batteries with

higher cell voltage and larger capacity, typical applications such as the equalization of power lead-acid battery. Energy is transferred through the symmetrical half-bridge structure with equalizing capacitors as the medium. The paper gives the necessary theoretical analysis of the capacitor charge and discharge process in the equalization system. A prototype of the equalization circuit was made to verify the method proposed in this paper, the test results prove the rationality and high efficiency of the proposed symmetrical half-bridge switch structure and corresponding drive circuit. Compared with the traditional complicated power switch driving method, the power switch driving circuit proposed in the paper is more stable and the control method is simpler.

REFERENCES

- [1] Torkashvand M, Khodadadi A, Sanjareh M B, et al.: 'A life Cycle-Cost Analysis of Li-ion and Lead-Acid BESSs and Their Actively Hybridized ESSs with Supercapacitors for Isolated Microgrid Applications', IEEE Access, 2020, pp. (99):1-1.
- [2] Dam S K, John V.: 'A Modular Fast Cell-to-Cell Battery Voltage Equalizer', IEEE Transactions on Power Electronics, 2020, pp. (99):1-1.
- [3] Irdawati Y, Sutanto H, Anam C, et al.: 'Silicone rubber with lead-acid composite as alternative radiation filter in digital radiography (DR)', Journal of Physics: Conference Series, 2020, 1505(1):012035 (7pp).
- [4] Wang W, Yao W, Chen W, et al.: 'Communication—Characteristic Charge Transfer Resistance of Electrodes on Lead-Acid Batteries', Journal of The Electrochemical Society, 2020, pp. 167(4):040515.
- [5] Chen, Yang, Shiyan, et al.: 'A MultiWinding Transformer Cell-to-Cell Active Equalization Method for Lithium-Ion Batteries With Reduced Number of Driving Circuits', IEEE Transactions on Power Electronics, 2016.
- [6] Lavety S, Keshri R K, Chaudhari M A.: 'Evaluation of Charging Strategies for Valve Regulated Lead-Acid Battery', IEEE Access, 2020, 8:164747-164761.
- [7] Wang P, Zhu C.: 'Summary of Lead-acid Battery Management System', IOP Conference Series: Earth and Environmental ence, 2020, pp. 440(2):022014.
- [8] Huang C.: 'Research on battery pack dynamic equalization technology with improved flying capacitor', International Journal of Low-Carbon Technologies.
- [9] Duan J, Duan M, Zhang K, et al.: 'Research on voltage equalization among multiple supercapacitor modules based on multiwinding transformer', International Journal of Electrical Power & Energy Systems, 2020, 120:106031.
- [10] Dam S K, John V.: 'A Modular Fast Cell-to-Cell Battery Voltage Equalizer', IEEE Transactions on Power Electronics, 2020, pp(99):1-1.
- [11] Satpathy P R, Sharma R.: 'Power recovery and equalization in partially shaded photovoltaic strings by an efficient switched capacitor converter', Energy Conversion & Management, 2020, 203(Jan.):112258.1-112258.21.

Author Index

H

Huipin Li 10

J

Jifeng Qu 10

Junfan Wang 10

K

Ka Wai Eric Cheng 5

M

Mingyu Gao 10

Minghao Wang 10

X

Xiaodi Zhang 1

Xiangdang Xue 5

Y

Yulong Fan 5

Submission Details

Only online submission will be accepted. Please first register and submit online. The paper is in double-column and is similar to most IET or IEEE journal formats. There is no page limit. Any number of pages of more than 6 will be subjected to an additional charge.

The paper guidelines can be downloaded using the link: <http://perc.polyu.edu.hk/apejournal/>

Any queries, please contact Prof. Eric Cheng, Publishing Director of APEJ, Dept. of Electrical Engineering, The Hong Kong Polytechnic University, Hung Hom, Hong Kong. Email: eeecheng@polyu.edu.hk Fax: +852-2330 1544

Any secretarial support and production related matters, please contact Dr. James Ho, Power Electronics Research Centre, The Hong Kong Polytechnic University, Hung Hom, Hong Kong. Email: eeapej@polyu.edu.hk Tel: +825-3400 3348 Fax: +852-3400 3343

Publication Details

The journal will be published 2-3 times a year. The first issue was published in 2007. Response time for paper acceptance is within 3 months.

Financial Charge

All the accepted papers will be printed without charge for 6 or less pages. An additional page charge is HK\$100 per page. A hardcopy of the journal will be posted to the corresponding author free of charge. Additional copies of the journal can be purchased at HK\$200 each. The charge includes postage and packing.

All Chinese Papers will be subjected to a translational fee of HK\$350 per page. It will be charged when the paper is accepted for publication.

Advertising

Advertisement is welcome. Full page advertisement is HK\$1000. For colour advertisements, the amount is doubled. All the advertisements will be both posted online in the journal website and hardcopy of the journal.

For advertising enquires and details, please contact Ms. Anna Chang, eeapej@polyu.edu.hk.

Tel: +852-3400 3348, Fax: +852-3400 3343

For payment, please send your cheque, payable to 'The Hong Kong Polytechnic University, address to Ms. Kit Chan, Secretary of APEJ, Dept. of Electrical Engineering, The Hong Kong Polytechnic University, Hung Hom, Hong Kong.'